Supplementary material for Journal of Fluid Mechanics

Microbubble formation by flow-focusing: role of gas and liquid properties, and channel geometry

Sarah Cleve[1,†], Anne Lassus[2], Christian Diddens[1], Benjamin van Elburg[1], Emmanuel Gaud[2], Samir Cherkaoui[2], Michel Versluis[1], Tim Segers[3], and Guillaume Lajoinie[1]

[1]Physics of Fluids group, Max Planck Univ. Twente Center for Complex Fluid Dynamics, Technical Medical (TechMed) Center, University of Twente, P.O. Box 217, 7500 AE, Enschede, THE NETHERLANDS
[2]Bracco Suisse S.A., Route de la Galaise 31, 1228 Plan-les-Ouates, SWITZERLAND
[3]BIOS/Lab on a Chip group, Max-Planck Univ. Twente Center for Complex Fluid Dynamics, MESA+ Institute for Nanotechnology, University of Twente, P.O. Box 217, 7500 AE, Enschede, THE NETHERLANDS
[†]now at: Univ. Lille, CNRS, Centrale Lille, Univ. Polytechnique Hauts-de-France, UMR 8520 - IEMN Institut d'Électronique de Microélectronique et de Nanotechnologie, 59000 Lille, FRANCE

1 Experimental results: different gases for the bubble production in the short channel

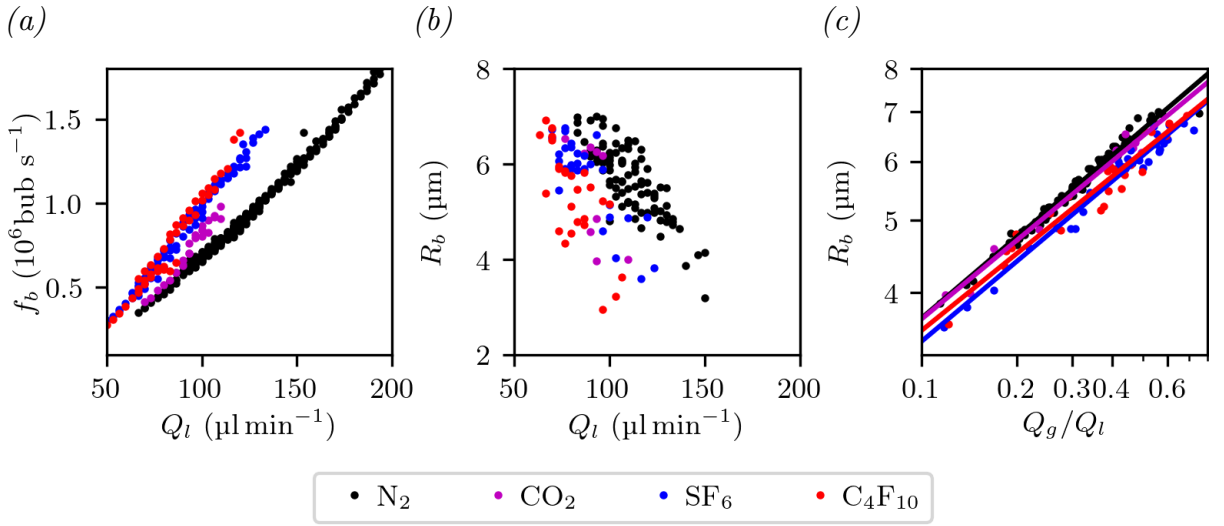

Figure S1: Experimental results for four different gases used for bubble production in the short channel. The liquid phase is the same in all experiments: water with the DSPC/DPPE-PEG5000 mixture. The production rate and bubble size as function of the liquid flow rate are shown in *(a,b)*, respectively. *(c)* shows he bubble size with respect to the flow rate ratio including a fit of a power law. The data shows the same trend as Fig. 4 in the main document for the long channel.

2 Experimental results: bubble production with Pluronic

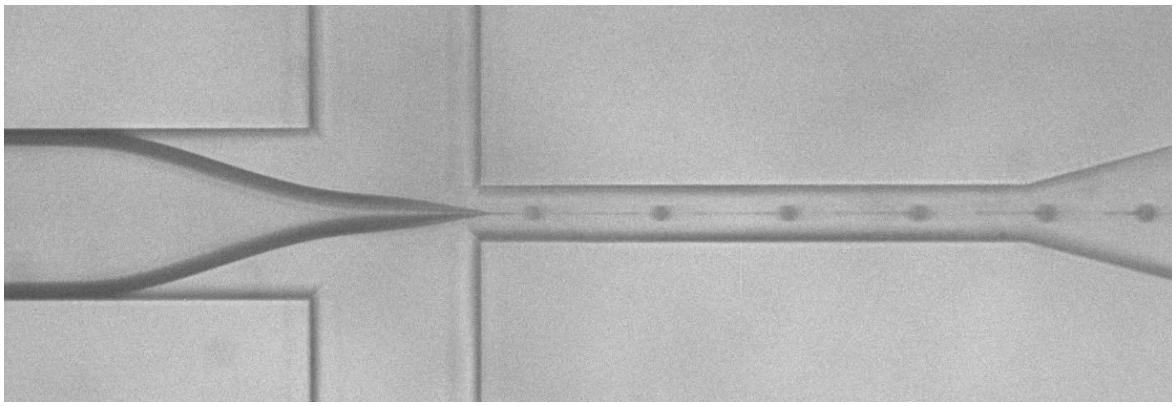

Figure S2: Example of bubble production with Pluronic F68. The effect visible here, of sub-µm filaments attached to the formed bubbles, only appears at a small parameter range. The gas filament is created behind the bubble and shortens along the channel. It shows resemblance with the inverse case of dripping of slender viscoelastic liquid filaments as reported by [Sen *et al.* (2021), 929, JFM]

3 Discussion: gas pressure and different flow-focusing geometries

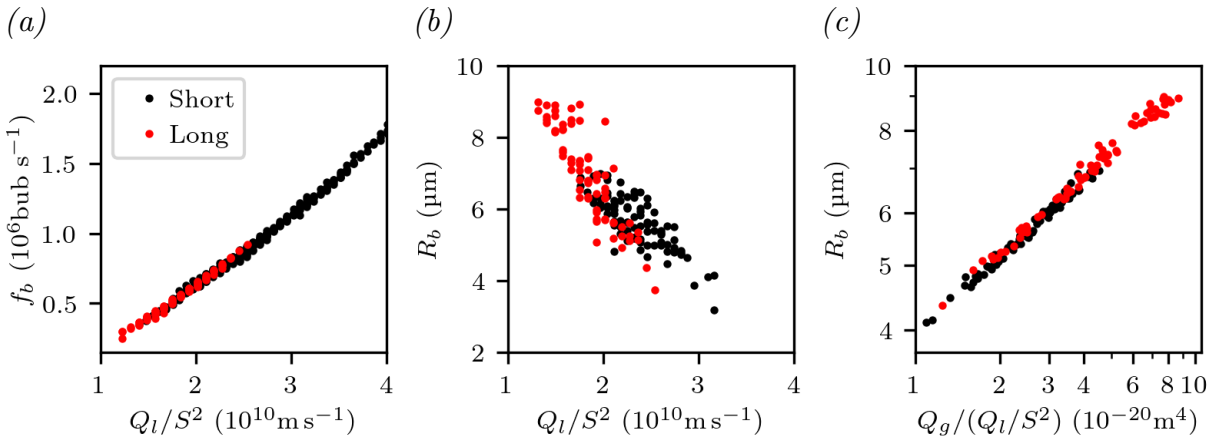

Figure S3: Data from Fig. 2 in the main document with an additional correction factor $1/S^2$ (square of the channel surface area) on the liquid flow rate leads to a perfect superposition between data from the short and the long channel.

As discussed in our previous paper [Cleve *et al.* (2021), 114202, PR Fluids] the pressure in the inlet region and the linear pressure loss along the channel scale as

$$\Delta p \sim \rho_l U^2 \sim \rho_l Q_l^2/S^2,$$
$$dp/dx \sim \mu_l (Q_l + Q_g)/(D - R^{*2})^2 \underset{\text{neglect gas}}{\sim} \mu_l Q_l/S^2,$$

respectively. Here, R^* was a correction factor for the bubble size. For further simplifying the discussion, we neglect the presence of the gas phase, which we have shown to be justified for small bubbles.

4 Numerical simulations: increased gas density

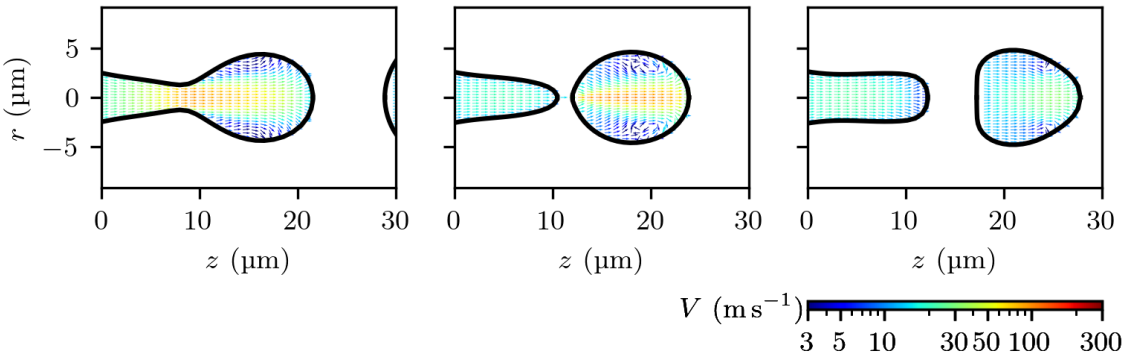

Figure S4: Zoomed in version of Fig. 9*(c)* from the main document to highlight the recirculation zones.

5 Comparison to theory: error of theoretical prediction

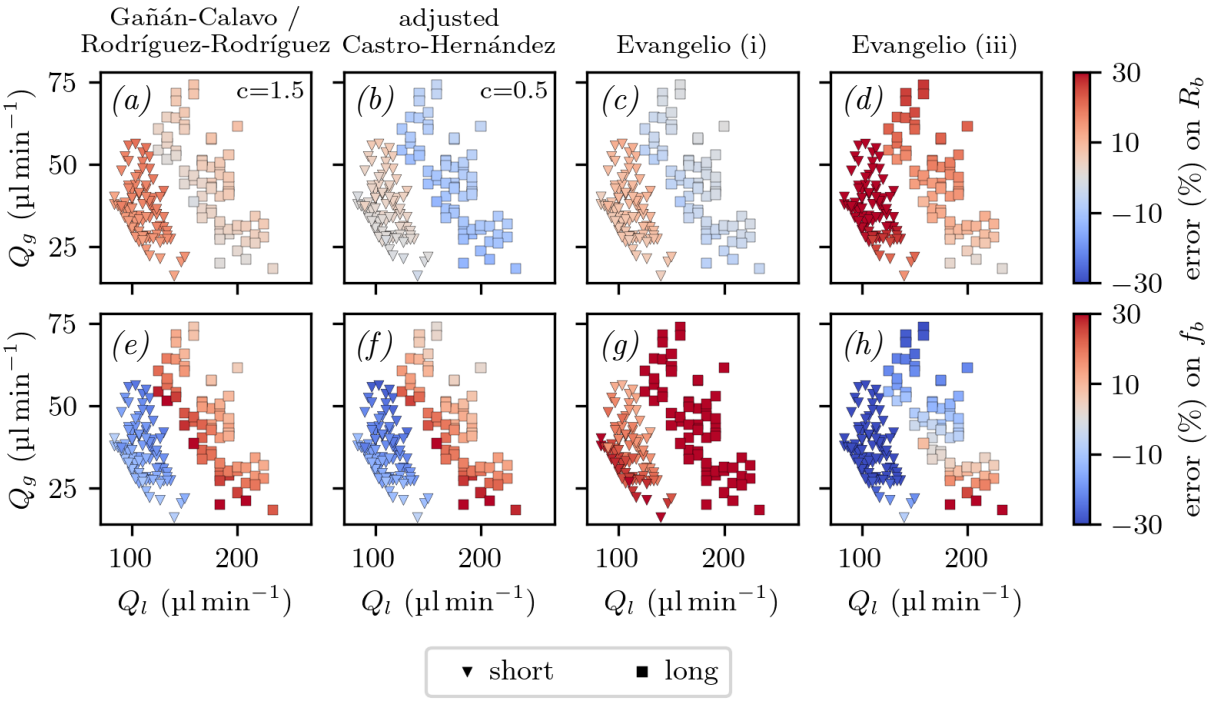

Figure S5: Comparison of our reference data (Fig. 2 in the main document) for the short and long channel with models from literature. Instead of the presentation $R_{\text{calculated}}$ versus R_{measured} and $f_{\text{calculated}}$ versus f_{measured} of Fig. 13 in the main document, we present here the error between the two models with respect to the experimentally used liquid and gas flow rates. The theoretical prediction gives a perfect match with experiment for the white points, overestimates the experimental data for red data points and underestimates them for blue data points.

6 Comparison to theory: adapted channel size

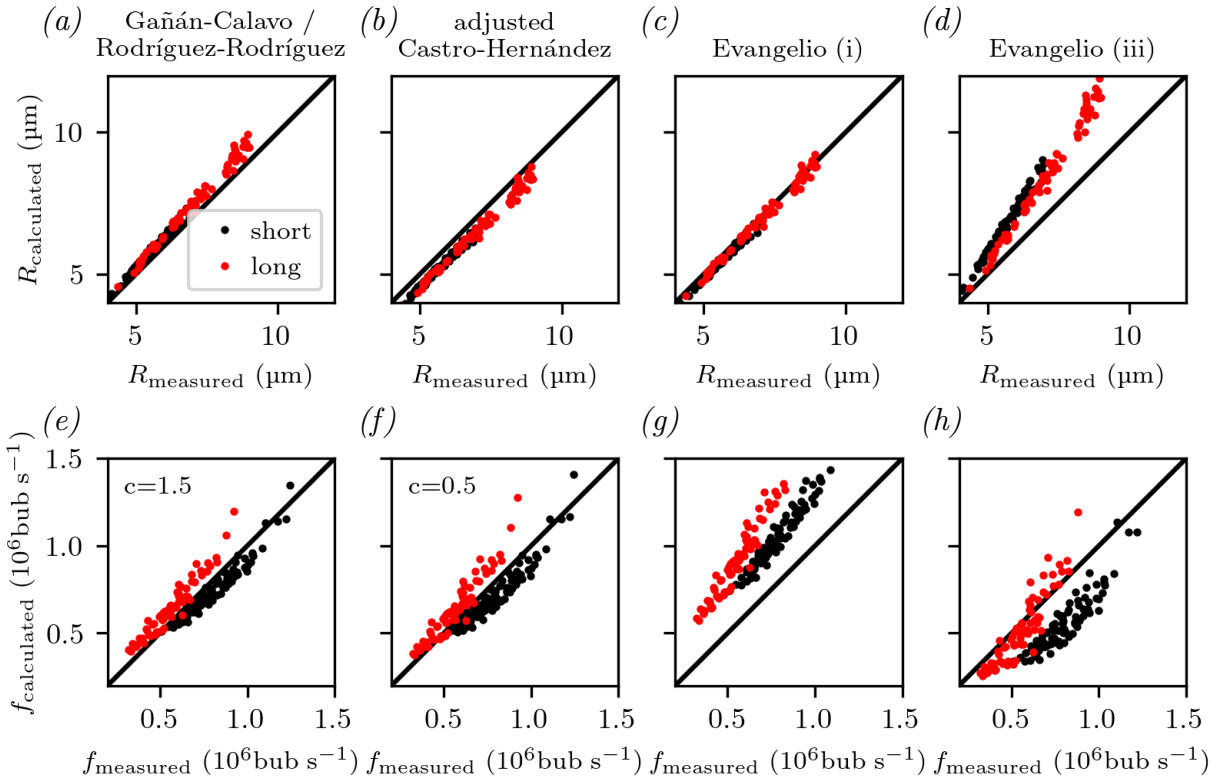

Figure S6: Comparison of our reference data (Fig. 2 in the main document) for the short and long channel with models from literature. This plot presents the same data as Fig. 13 in the main document, but for this plot we assume that the diameters of the channel section are $d_{small} = 17\,\mu m$ and $d_{large} = 23\,\mu m$.

7 Comparison to theory: long channel

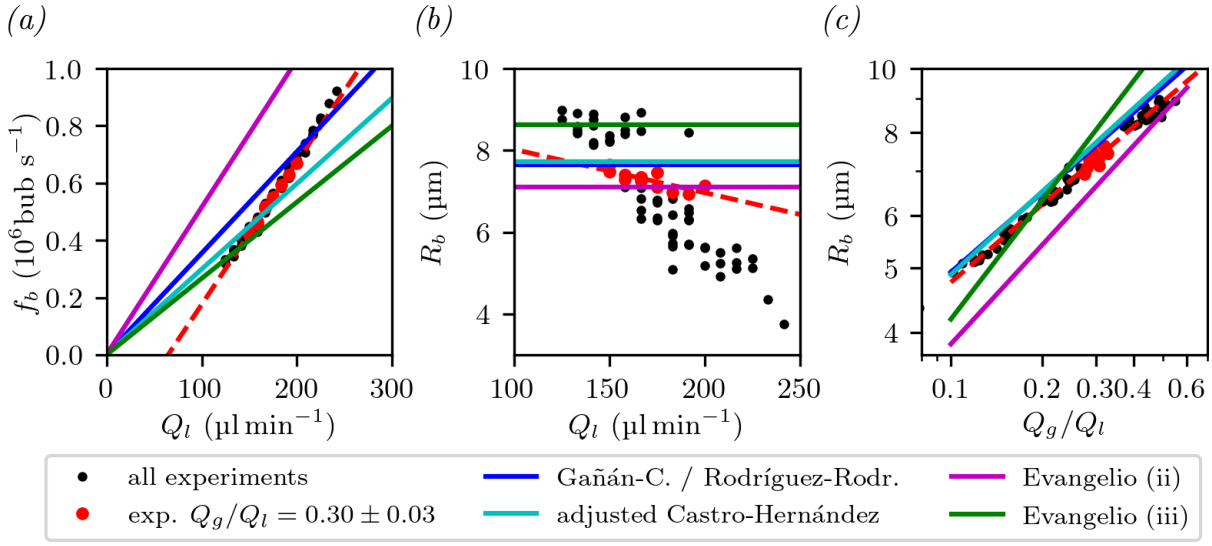

Figure S7: Comparison of our reference data (Fig. 2 in the main document) for the long channel with models from literature. Each panel shows experimental data (black data points), experimental data for the range $0.27 < Q_g/Q_l < 0.33$ (red data points), a linear fit through these points, and different theoretical predictions (with $Q_g/Q_l = 0.3$ fixed for *(a,b)*). *(a)* Production rate as a function of the liquid flow rate. For the adjusted Castro-Hernandez model we have multiplied the bubble size by a factor 0.5 in order to fit to our results. *(b)* Bubble size as a function of the liquid flow rate. *(c)* Bubble size as a function of the gas to liquid flow ratio. The same trends as for the short channel (Fig. 14 in the main document) can be observed.

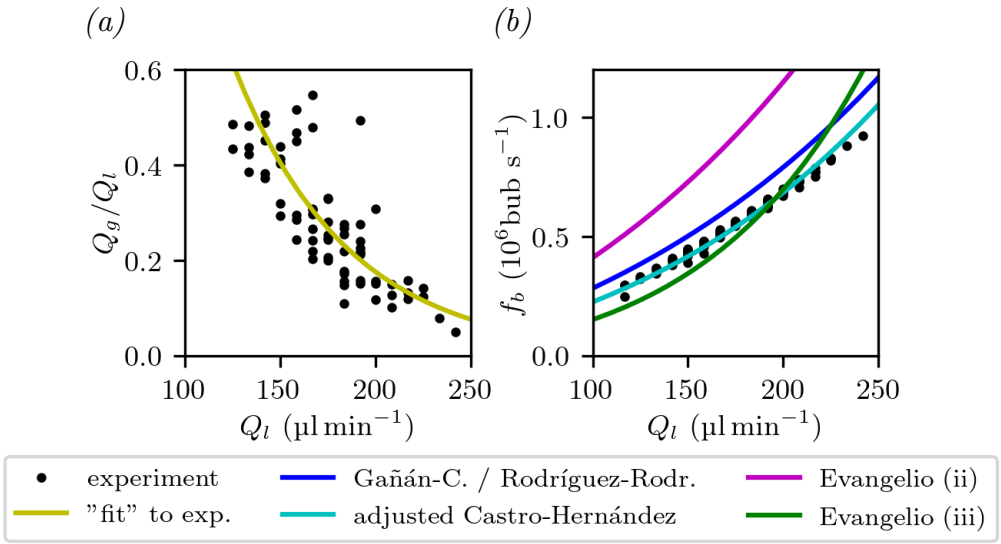

Figure S8: For the long channel: *(a)* Gas to liquid flow rate ratio as a function of the liquid flow rate. A trend line is fitted to data. *(b)* Production rate as a function of the liquid flow rate. The experimental data is compared to the theoretical models, in which we applied the trend line from panel *(a)* for the ratio $Q_g/Q_l(Q_l)$. The same trends as for the short channel (Fig. 15 in the main document) can be observed.